Appl. Phys. A 77, 223–228 (2003)
DOI: 10.1007/s00339-003-2143-3

Applied Physics A
Materials Science & Processing

D. ASHKENASI[1,✉,*]
G. MÜLLER[1]
A. ROSENFELD[2]
R. STOIAN[2]
I.V. HERTEL[2]
N.M. BULGAKOVA[3]
E.E.B. CAMPBELL[4]

Fundamentals and advantages of ultrafast micro-structuring of transparent materials

[1] Laser- und Medizin-Technologie GmbH, Schwarzschildstr. 8, 12489 Berlin, Germany
[2] Max Born Institut, Max-Born-Str. 2a, 12489, Germany
[3] Institut of Thermophysics SB RAS, Novosibirsk, Russia
[4] Göteborg University and Chalmers University of Technology, Göteborg, Sweden

Received: 17 January 2003/Accepted: 8 February 2003
Published online: 28 May 2003 • © Springer-Verlag 2003

ABSTRACT Experimental investigations using femtosecond and picosecond laser pulses at 800 nm illuminate the distinctions between the dynamics and nature of ultrafast processing of dielectrics compared with semiconductors and metals. Dielectric materials are strongly charged at the surface on the sub-ps time scale and undergo an impulsive Coulomb explosion prior to thermal ablation. Provided the laser pulse width remains in the ps or sub-ps time domain, this effect can be exploited for processing. In the case of thermal ablation alone, the high localization of energy accompanied by ultrafast laser micro-structuring is of great advantage also for high quality processing of thin metallic or semiconducting layers, in which the surface charge is effectively quenched.

PACS 79.20.Ds

1 Introduction

The availability of ultrashort sub-ps pulsed lasers has stimulated a growing interest in exploiting the enhanced flexibility of femtosecond technology for micro-machining. Ultrashort laser pulses (USLP) offer a variety of advantages for precision micro-fabrication. Due to lower energetic thresholds for sub-picosecond ablation and the controllability of individual laser pulses (e.g. by laser pulse duration), the amount of energy deposited into the processed sample can be minimized and highly localized. This leads to a reduction of unwanted thermal effects, so that very clean microstructures can be achieved with optimized pulses. Also non-linear optical effects can be exploited. Self-focusing due to the non-linear optical Kerr effect may be used to induce long narrow 3d-modification traces in the bulk of wide band-gap materials. Laser drilling of high-aspect-ratio micrometer-thin channels with ultrashort laser pulses has been demonstrated, utilizing the advantages in the high ablation rates combined with a relatively low heat deposition [1, 2].

Concomitantly, an increased interest in probing the nature of excitation has been stimulated. This includes the dynamics of energy redistribution in irradiated solids and the precursor mechanisms for material removal [3–5]. The initiating excitation mechanism is believed to be multi-photon absorption, either from already present morphological or structural defect states in the band gap or by interband transitions. In a real crystal, complex multi-photon transition routes seed the conduction band with free carriers, increasing the plasma density of the dielectric. Additional photons in the laser pulse enhance the free-electron heating process with additional ionization due to electron impact [1]. This is accompanied by photoelectron emission with surface charging and thermalization of the quasi-free electronic system on a material-dependent time-scale. Energy transfer to the lattice by electron–phonon coupling follows with subsequent heating of the sample [6]. Recently, the observation of fast ions in the initial gentle etch phase [7] of femtosecond laser ablation of sapphire has been reported, in which ions of different mass have the same momenta, which scales only with the carried charge. This was interpreted as originating from an impulsive macroscopic Coulomb explosion (CE) of the charged dielectric surface [8].

2 Fundamental aspects in the dynamics of ultrashort laser ablation

The dynamics of the initial stages of excitation in solids leading to charging, heating, and material expulsion was explored using pump–probe laser techniques and charged particle detection to emphasize the material-dependent competition between non-thermal and thermal mechanism [8]. The positive ion and electron emission was monitored as a function of the delay between two sub-threshold 100-fs 800-nm laser pulses. Comparing the results for metals, semiconductors, and dielectrics, it was confirmed that the CE mechanism is only significant for dielectrics [9]. Pump–probe measurements for both prompt electron and Al^+ production for Al_2O_3 are shown in Fig. 1. The ion data were obtained by choosing two different velocity windows in the time-of-flight mass spectrometer for the detected ions and scanning the pump–probe delay in both cases. The pump–probe signal from the faster ions (squares) shows a double-peak structure, illustrating the competition between the different mechanisms. The slower ions (circles) have a single broad peak at 20 ps. It can be seen from Fig. 1b that the prompt electron pump–probe data (electrons generated by photoemission) correlate very well with the first peak in the fast ion signal, indicating that prompt photoemission is indeed the origin

✉ Fax: +49-30/670-53-500, E-mail: d.ashkenasi@lmtb.dt
**Present address:* LMTB GmbH, Berlin, Fabeckstr. 60–62, D-14195 Berlin, Germany

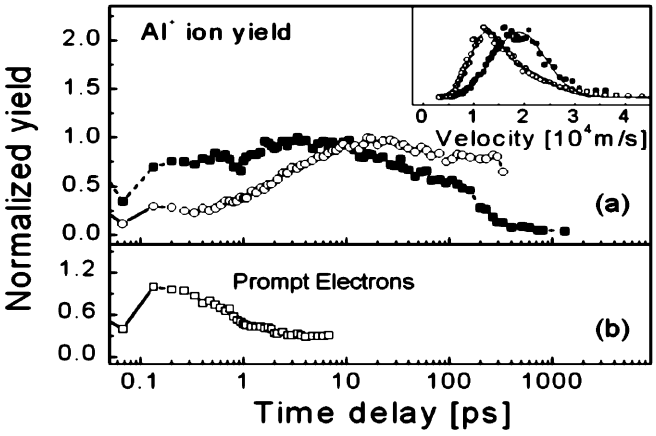

FIGURE 1 Pump–probe measurement of Al_2O_3: **a** Al^+ yield as a function of time delay between two equal sub-threshold 100-fs laser pulses at 800 nm. *Squares*: "fast" ion signal with a velocity of 2×10^4 m s^{-1} demonstrating a double-peak structure. *Circles*: "thermal" ion signal with a velocity of 1.2×10^4 m s^{-1}. *Inset*: Al^+ velocity distribution for two delays: 12 (*circles*) and 0.6 ps (*squares*); **b** Prompt electron signal under identical pump–probe conditions as in **a**

of the observed ion CE. The first results show that sufficient charge can be accumulated at the dielectric surface to initiate Coulomb explosion on the 100-fs time-scale. With semiconductors and metals, the higher electron mobility and higher density of available free electrons ensures effective screening and a much smaller net positive charge accumulated during the laser pulse. This accumulated charge is not sufficient, by orders of magnitude, to induce a macroscopic electrostatic break-up of the outer layers of the substrate.

To explain the observed behavior, we have calculated the electronic dynamics including surface charging effects for Al_2O_3, Si, and Au. The bulk substrate is divided into layers each of depth 0.5 nm and the time dependence of charging and relaxation is calculated for each layer using appropriate boundary conditions. For the purposes of these calculations, we are mainly interested in the induced charge at the outer layer of the bulk material. We use a slightly different approach for metals compared with dielectrics and semiconductors. For Al_2O_3 we write the continuity equation for free electrons excited by the 800 nm laser pulse as

$$\frac{\partial n_\mathrm{e}}{\partial t} + \frac{1}{\mathrm{e}}\frac{\partial J}{\partial x} = \left(\sigma_6 I^6 + \alpha n_\mathrm{e} I\right)\frac{n_\mathrm{a}}{(n_\mathrm{a}+n_\mathrm{i})} - R_\mathrm{e} - PE, \qquad (1)$$

where $\sigma_6 I^6$ is the rate of multi-photon ionization, n_x is the density of particles (a: neutral atoms, i: positive ions, e: electrons), I is the laser intensity, J is the electric current density, $\alpha n_\mathrm{e} I$ is the avalanche term, R_e is the recombination term, and PE is photoemission. The rate of multi-photon ionization and the avalanche coefficient were based on a fit to the experimental results for the optical damage thresholds at different pulse durations [10] following a similar approach to Stuart et al. [11] (taking also into consideration the observed decay in the threshold electron density at longer pulse durations [12]) and estimated for Al_2O_3 with $\sigma_6 = 8 \times 10^9$ cm^{-3} ps^{-1} (cm^2/TW)^6 and $\alpha = 6$ cm^2/J.

The spatially and temporally dependent laser power inside the dielectric is determined by the optical response of a free electron plasma and the vacuum–plasma interface, being given by the complex dielectric function and Fresnel formulas [11, 13] with a damping term $\omega\tau = 3$ to match the observed reflectivity of 70% for supercritical electron densities [14]. We consider a statistical distribution of free electronic momenta in a dielectric, in which the vacuum level is close to the conduction band minimum, thus facilitating ionization. Only electrons with a momentum component normal to and in the direction of the surface can escape. This assumption is justified for most dielectrics such as a-SiO_2, in which the vacuum level is approximately 1.1 eV above the conduction band [15]. Thus, we assume that, on average, half of the free electrons produced by multi-photon ionization and avalanche are immediately photo-emitted from a layer near the surface. Maximum photoemission occurs from the surface and decreases exponentially towards the bulk giving a photoemission term

$$PE = \frac{1}{2}(\sigma_6 I^6 + \alpha n_\mathrm{e} I)\frac{n_\mathrm{a}}{(n_\mathrm{a}+n_\mathrm{i})}\exp\left(-\frac{x}{l}\right), \qquad (2)$$

with the electron escape depth $l = 1$ nm [16].

The ion density is given by a similar equation as (1) disregarding photoemission, and the electric current density is put in a relevant form dominant in the depletion region as

$$J = -\mathrm{e}n_\mathrm{e}\mu_\mathrm{e}E - \mathrm{e}D\nabla n_\mathrm{e}, \qquad (3)$$

with the electron mobility $\mu_\mathrm{e} = 3 \times 10^{-5}$ m^2/(V s) (ten times lower than that reported by Hughes [17] for a better match to the measured diffusivities [18]). The drift term was calculated using the Poisson equation. Since we consider transport in the local electric field, calculated from the Poisson equation, plasma-screening effects within the bulk material are automatically accounted for. The diffusion coefficient $D = k_\mathrm{B}T_\mathrm{e}\mu_\mathrm{e}/\mathrm{e}$ is considered negligible for dielectrics compared with semiconductors and metals.

The same approach was used for Si, for which both one and two-photon ionization was considered. The cross-sections for photoionization and the reflection coefficient were taken into account [13]. An equation for hole generation and consideration of both the electron and the hole current density was included into the calculation ($\mu_\mathrm{e} = 0.15$ m^2/(V s); $\mu_\mathrm{h} = 0.045$ m^2/(V s)). The photoemission term was treated analogously to that for metals [19, 20] (see below). The metallic case is considered as a plasma with a supercritical electron density. The system of equations used to describe the electric field generation consists of the heat flow equation for electrons (4) (lattice coupling was neglected on this short time scale) [21], the equation for the electric current density, the continuity equation (1) without source/sink terms, and the Poisson equation:

$$\frac{C_\mathrm{e}}{T_\mathrm{e}}\left(\frac{\partial}{\partial t}T_\mathrm{e}^2 + \frac{J}{\mathrm{e}n_\mathrm{e}}\frac{\partial}{\partial x}T_\mathrm{e}^2\right) = \frac{K_{\mathrm{e},0}}{T_\mathrm{l}}\frac{\partial^2}{\partial x^2}T_\mathrm{e}^2 + 2S(x,t), \qquad (4)$$

where T_e and T_l are the electron and lattice temperatures, respectively, C_e is the electron heat capacity, $K_{\mathrm{e},0}(T_\mathrm{e}/T_\mathrm{l})$ is the thermal conductivity of the electrons, and the energy source term S is as given in [21]. The photoemission condition takes into account a 3-photon electron emission process [19].

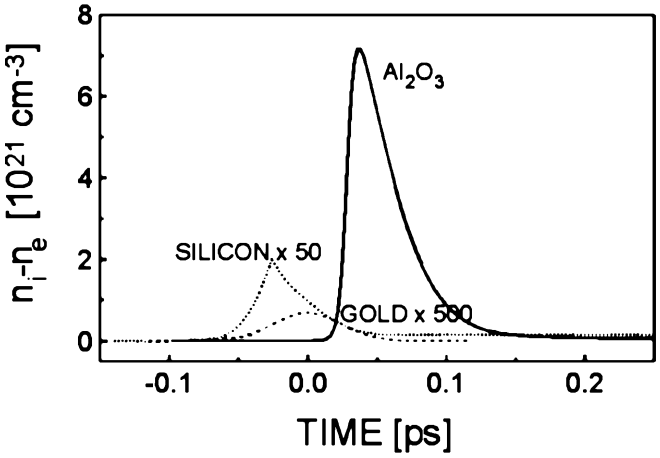

FIGURE 2 Calculation of net surface charge density as a function of time for a laser fluence slightly above the single shot ion emission threshold for each material. Laser pulse is centered at $\tau = 0$ fs (FWHM = 100 fs). Note the change in density scales

The build-up of net positive charge on the surface of each target as a function of time is plotted in Fig. 2. The Gaussian laser pulse is centered at $t = 0$ with a FWHM of 100 fs. The laser fluence used to calculate the charging dynamics are slightly above the experimental ablation threshold [10, 13]. It is clear that the net charge is much larger for the dielectric target than for the metal or semiconductor. It is also time-retarded, instead of roughly following the laser pulse envelope as for metals and semiconductors. If we estimate the magnitude of the electric field at the surface of Al_2O_3, due to the net accumulation of positive charge, and assume that this field exists for 50 fs (FWHM), we can assess the velocity with which the Coulomb-exploded Al^+ ions are emitted from the surface based on momentum conservation laws. This is 2.3×10^4 m s^{-1}, in excellent agreement with the experimentally determined values for Al_2O_3 [6].

3 Examples of micro-processing with ultrashort laser pulses

3.1 *Surface Coulomb explosion and thermal ablation phases in c-Al_2O_3*

A suitable choice of laser parameters can tune the transition between different processes, dominated by either non-thermal or thermal mechanisms, respectively. This change of mechanisms, which is attributed to different ablation phases, is most evidently identified by the visual appearance of the irradiated area in a scanning electron microscope (SEM) detection. This is illustrated in Fig. 3 for different numbers of shots per site (N) at constant fluence. The first laser shots above the damage threshold initiate the *gentle etch phase*. For 200-fs irradiation, the gentle etch-phase ($N < 30$) is characterized by an extremely smooth surface (sometimes even smoother than the initial state), both at the side-wall and at the bottom of the dip, with almost no pattern developing except ripples [1] and with no debris particles around the rim. The ablation rate is low, around 20–30 nm/pulse, as determined by a volume evaluation using AFM [7]. The ripple modulation depth is also approximately 30 nm, comparable with the ablation rate per shot. It is believed that

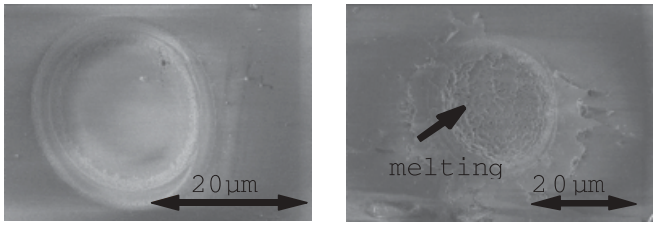

FIGURE 3 Transition from gentle to strong etch phase in c-Al_2O_3 irradiated by 200-fs laser pulses

interference between incoming and scattered light on the surface generates an interference pattern, impinging on the spatial distribution of excited electrons in the conduction band. Material is removed with every laser pulse, including the first one.

At a higher number of laser pulses, the appearance of the spot changes dramatically, as illustrated for $N = 30$ in Fig. 3. The surface shows the characteristics of the *strong ablation phase*: increased roughness and signs of a violent process of a thermal nature, including droplets, melting traces, and splintered edges. At a still higher number of shots, crater formation is observed. The mechanisms underlying this *strong etch phase* is basically thermal and may be associated with phase explosion [22, 23]. The change from the gentle to the strong etch phase occurs between 25 and 30 laser pulses per site at this particular fluence and depends also on the fluence and laser pulse-width. At the same time the ablation rate increases drastically ($\sim$ 300 nm/pulse) with an additional strong decrease in the ionization degree. This allows a determination of the cross-over between the two phases in a quantitative manner [24].

The strong electron photoemission drives an electrostatic breakup of a finite layer (ca. 3–5-nm thickness) with a dominant non-thermal character of the charged particles involved in the Coulomb material explosion. The gentle ablation appears as a consequence of energy absorption in the laser-induced electron plasma at almost solid density, localized within the non-linear absorption range. Therefore, in the gentle etch phase, the ablation is subject to non-thermal *and* to thermal mechanism(s). A discrimination between the two is demonstrated in the different dynamics. For repetitive irradiation, the defect-affected region is extended in volume. Non-linear excitation via defect states is more probable at larger optical penetration depths. In effect, this yields a magnitude higher ablation rate with a more dominant thermal character. The appearance of this strong ablation phase at a shot-number cross-over is a consequence of defect accumulation. The energy penetration depth for material removal increases significantly, leading to an overwhelming thermal contribution in the ablation, i.e. in the form of a phase explosion, in response to the homogenous nucleation of liquid bubbles near the critical thermodynamic temperature. The smoothing effect in the material removal based on Coulomb explosion (and in the "gentle" etch phase) can be utilized for the laser-polishing of dielectric surfaces. Preliminary studies performed at the Max Born Institute demonstrate the benefits in laser surface processing and refurnishing based on intensive photoelectron emission with ultrafast laser technology.

3.2 *Selective thermal removal of thin transparent layers with laser pulses*

Laser material structuring based on thermal mechanisms may lead to very good results in, for example, the surface mean roughness and processing quality, provided the energy penetration characterizing the thermal activation remains localized in the selected region. For semi-conductive and metallic materials, for example, thin films, the ablation processes are of a thermal nature under the discussed condition. Coulomb explosion, as in the case of sapphire, is not expected for conductive layers. A well-defined localization of photon energy is crucial for any high quality removal of one or several thin layer(s) from the substrate. The selective removal of only one single layer on a multi-layer system is a even more challenging, since thermal effects should remain confined [25, 26]. This is more true if these layers are transparent, since in the linear case, the optical penetration depth is usually large ($\gg 1\,\mu$m) compared with the typical layer thickness ($< 1\,\mu$m). The processing window in this case for a successful application yields a reduced choice in the appropriate wavelength–pulse width combinations available. At first glance one would recommend UV laser light for transparent thin layers. However, successful selective laser-induced removal of thin transparent layers using laser pulses in the IR was reported recently [27].

The processing experiments were conducted by focusing ultrashort laser pulses, generated by a Ti:sapphire laser system with chirped pulse amplification (Quantronix/Spectra Physics), on the sample with one or more layers using fused silica lenses with a focal length of 75 mm. In addition, low-power cw He-Ne laser light illuminated the region of interest on the sample to monitor possible changes in surface roughness during the (multi) pulsed processing. In situ inspection was achieved by enlarged visualization of the (pulsed laser-activated) surface by a combination of far-field microscope, CCD-camera, and video monitor. This allowed an on-line estimation of the damage threshold, which was determined with higher precision using ex situ methods. The variation of single pulse energy (i.e. laser fluence) was accomplished by means of an attenuator (Newport). A shutter was used for single laser shot control, i.e. N on 1 damage threshold studies, where N specifies the number of shots placed on the same spot under identical conditions at a repetition rate between 1 and 100 Hz. Processing of grooves and areas was performed at a 100- to 1000-Hz repetition rate [28]. As an example of laser processing of a single layer system, Fig. 4 depicts a 150-nm thin indium tin oxide (ITO) layer partly removed from a 1.1-mm-thick glass substrate using 3-ps laser pulses at a wavelength of 800 nm. Note that the linear absorption coefficient for ITO at 800 nm is $< 1\%$, compared with $> 80\%$ at 266 nm. The fairly well-defined edges of the resulting 150-nm-deep groove is outlined by a rim with a curl of only 20 nm. A further improvement in quality was observed after using sub-ps laser pulses at an equal wavelength. Atomic force analysis of the laser processed ITO layer reveals the following situation: at a fluence of $< 2\,\mathrm{J/cm^2}$ the first shot slightly roughens the surface. The second shot initiates the ablation, and additional shots remove any remaining ITO from the glass surface, depending on the fluence level. The AFM profile analysis suggests a linear

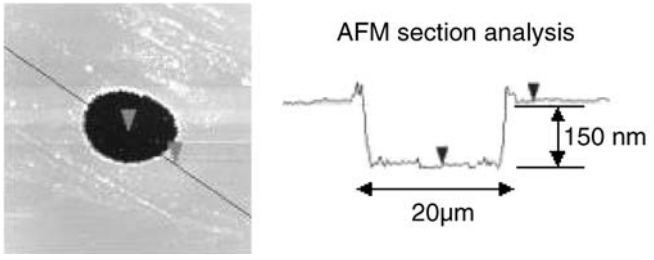

FIGURE 4 AFM analysis of a laser-induced micro-pocket after removal of ITO layer using 10 laser pulses at a wavelength of 800 nm, a pulse width of 3.6 ps and a single laser pulse fluence of ca. 1 $\mathrm{J/cm^2}$. The depth profile in the cross-section (*right*) illustrates the quality of removal

increase of ablated volume with increasing fluence. In other words, applying USLP at 800 nm even enables a partial removal of the 150-nm thin ITO layer. With UV laser pulses at a pulse width in the ns range, the processing quality is strongly reduced: a curl of several 100 nm to 1 µm is obtained, not adequate for most applications. Using UV laser pulses (266 nm) at a pulse width of 0.2 ps, the precision compared with the ns case is improved as expected, however, not to an extent above the processing quality using ultrashort laser pulses at 800 nm, as in the example shown in Fig. 4.

Figure 5 reveals a continuous rise in threshold with increasing pulse duration, a tendency also observed at a much higher fluence level for transparent dielectrics, e.g. glass or fused silica [28]. Specifically in the case of ITO (on glass), the results in Fig. 5 may be explained by an expected large optical penetration depth due to the minor linear absorption coefficient at 800 nm. Any form of efficient localization of laser energy can be explained only by invoking non-linear effects such as multi-photon absorption, which is more efficient at higher peak intensities, i.e. reduced pulse duration. The damage threshold for ultrashort laser pulses at 800 nm is less than 30% of the glass substrate (polished and uncoated). This ensures a wide fluence processing window for the removal of ITO from the glass substrate using ultrashort laser pulses in the IR. Thermal activation of the ablation process is predominant.

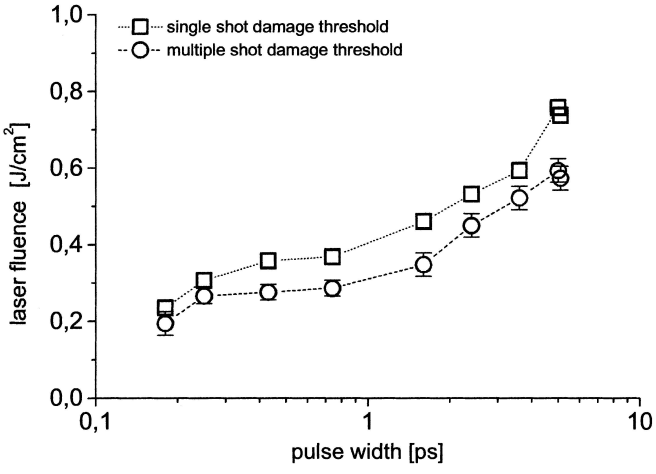

FIGURE 5 Single and multiple shot damage threshold for ITO on glass at 800 nm as a function of the laser pulse width

For ITO on glass we also performed processing experiments using only the oscillator system of the fs laser system. Focusing the fs laser pulses to a diameter below 3 μm at a single pulse energy of only 10 nJ and a repetition rate of 80 MHz, we obtain a complete and very precise removal of ITO from the glass substrate at fluence levels around only 100 mJ/cm^2. This drop in processing threshold – compared to the sub-1-kHz application – seems to have its origin in the reduced diffusion rate for 80-MHz processing, underlying our assumption of a predominant thermal activation in the material removal of ITO with fs laser pulses. However, to avoid any misunderstanding, the high peak power of the low-energy fs laser pulses is an absolute necessity for achieving a minimal free-electron plasma density as a precursor for additional (thermal) photon absorption on the surface (or inside) of the transparent layer. This case of localized energy accumulation is comparable to the fs high repetition laser-induced plasma reactions and modifications reported in bulk glass and fused silica at single pulse energies below 100 nJ [29].

Another example of selective thin layer processing is discussed in the following two layer case: 200-nm thin polyaniline (PANI) layer on a 1-μm-thick photo-resist film located on a glass substrate. PANI on glass shows a high absorption of 55% at 800 nm compared with the photo-resist on glass of less than 1%. At a wavelength of 266 nm the absorption coefficients are practically identical for both layers and reach levels above 80%.

Figure 6 depicts the laser threshold fluence for damage and ablation of a 200-nm thin PANI layer on a 1-μm-thick photo-resist on the 1.1-mm-thick glass substrate using ultrashort laser pulses at a wavelength of 800 nm and a pulse duration of 0.2 ps. In this case it is necessary to discriminate between the observation of increasing surface roughness (damage) and actual material removal (ablation). The former appears to be independent of the number of laser pulses. On the contrary, the ablation threshold drops sharply between a single shot and ten successive laser pulses. As the laser fluence is reduced below 20 mJ/cm^2 (1/4 of the single shot threshold fluence for ablation) no ablation is observed even after several thousand laser pulses. Laser fluence in an interval between the single shot threshold for damage and ablation leads to an increased roughening of the surface. This effect causes a reduction in the penetration depth at 800 nm and, hence, leads to a lower threshold for ablation. The damage and ablation thresholds for 800-nm and 5-ps laser pulses show an almost identical behavior as depicted in Fig. 6 for 0.2-ps laser pulses. In contrast to the ITO on the glass substrate, the threshold values are far less dependent on the pulse duration in the fs and ps range. Also, the damage threshold is approximately an order of magnitude lower for the PANI on the photo-resist compared with the single layer ITO sample. The low damage threshold and the nature of the modification prior to (complete) removal of the PANI layer is indicative of optical absorption or thermal activation mainly at the interface between the PANI and the photo-resist. Damage seems to have its origin at the rear side of the PANI layer. Sub-layer removal of PANI as in ITO on glass was not achieved.

Figure 7 depicts six processing examples of the sample 200-nm PANI on 1-μm photo-resist on a 1.1-mm glass substrate using ultrashort laser pulses at 0.2 ps and 800 nm. The top left laser-induced modification at 44 mJ/cm^2 and $N = 1$ laser shot illustrates the first signs of surface roughening at a fluence level just above the damage threshold. After a second laser shot at an equal fluence of 44 mJ/cm^2 (top-middle of Fig. 7) the optical impression suggests an increase in surface roughening. A third laser shot finally yields additional roughening and localized partial removal (ablation) of the transparent PANI layer. The photo-resist layer remains unaltered, as verified by high-resolution profile analysis of these structures. For single shot processing at a laser fluence of 50 mJ/cm^2 one observes additional surface roughness in size and depth (middle left picture of Fig. 7) compared with the lower fluence case, still without removing the top PANI layer from the photo-resist. Selective removal at $N = 1$ actually starts at a fluence level above 100 mJ/cm^2, beginning in the center region of the focused laser beam (bottom-left picture of Fig. 7). In the picture at the bottom-right of Fig. 7, we present an example of the successful removal of the 200-nm PANI layer

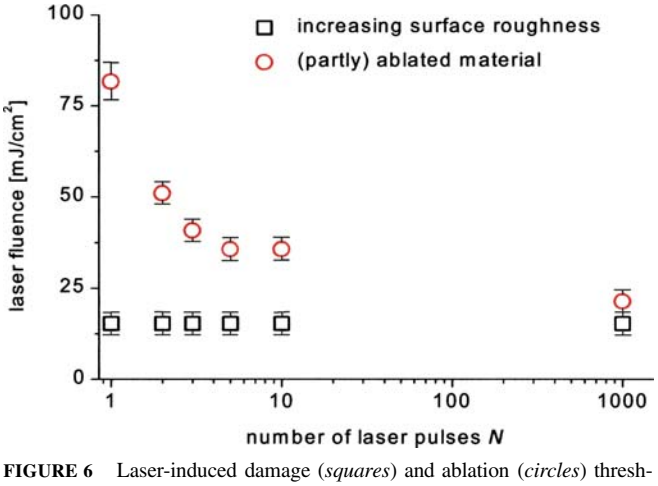

FIGURE 6 Laser-induced damage (*squares*) and ablation (*circles*) threshold of PANI (on photo-resist on glass) at a wavelength of 800 nm and a pulse width of 0.2 ps as a function of the number of laser shots N per location

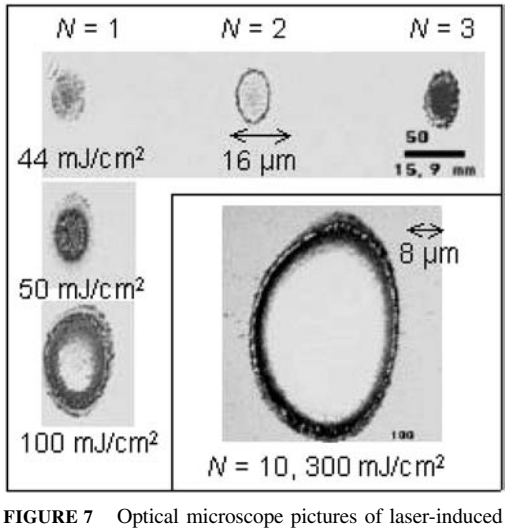

FIGURE 7 Optical microscope pictures of laser-induced modifications on the multi-layer system II: PANI on photo-resist on glass using fs laser pulses at 800 nm. N: number of laser shots. The laser fluence of 44 mJ/cm^2 was used to generate the top three modifications

after 10 laser shots at a laser fluence of 300 mJ/cm^2. We observe a transition from a dark to a light optical impression in the center of illumination corresponding to the surface of the photo-resist. The photo-resist film itself is not removed, not even partially. The mean roughness inside the processed surface area, i.e. the unconfined photo resist, equals that of the original coating, unless the laser fluence is tuned above 500 mJ/cm^2. One drawback in the application is an increased elevation of 50 nm at the rim of the processed area, as illustrated in a dark line between the unaffected and the ablated region (Fig. 7). This effect may be reduced by introducing a "top-hat" profile in the processing beam, instead of a Gaussian intensity distribution. The modifications are surprisingly reproducible, considering the significant changes obtained by slight adjustments in the laser fluence. Also, the results for the wavelength–pulse duration combination of 800 nm and 5 ps are equivalent to the fs case, with a slight tendency to increase the rim elevation. In the near IR region, fs laser pulses appear to be superior to the ps pulses with regard to the quality of the irradiated area as well as the ablation efficiency.

In contrast to the removal of ITO on glass, the choice of the wavelength is much more crucial when it comes to the ablation of PANI on photo-resist on glass. A selective removal using ultrashort UV laser pulses (266 nm/0.2 ps) was not obtainable. The variation of the laser fluence and number of shots under this condition demonstrated a complete removal of PANI with the photo-resist, as confirmed by determination of the depth profiles for the processed multi-layer system. The material reaction in the damage stage in the form of surface roughening, acting as a pre-cursor of ablation, establishes "optical windows" for the laser light to penetrate into the lower layer, the photo-resist. Additional laser pulses may then interact very strongly with the second layer. Using ultrashort laser pulses in the IR, this effect is much less significant, since the linear absorption coefficient of the photo-resist layer is very low. This result is quite the opposite to the UV case, in which the high linear absorption coefficient of the photo-resist leads to the observed non-discriminative damage and ablation in both layers. In other words: even though the wavelength–pulse width combination of sub-ps and UV is generally believed to have several advantages, such as efficient localization of photon energy, high ionization probability and significant potential for non-thermal ablation as CE, this study has proven that this combination is not the number one choice for processing certain delicate multi-layer systems.

4 Summary

In conclusion, we have studied, both experimentally and theoretically, the dynamics of electronic and lattice excitation and material removal in ultrafast laser ablation of dielectrics, semiconductors, and metals. Different dynamical behaviors are observed, which have important consequences for the mechanisms of material removal. In particular, it is possible to obtain a very high charging of dielectric surfaces, which can lead to a macroscopic Coulomb explosion of the top surface layers. The calculations are in good agreement with fs pump–probe studies and measurements of velocity distributions of emitted ions. Concerning possible applications, a comparison of ultrashort laser pulse processing for dielectric surfaces and thin conductive transparent layers is discussed. For the laser-induced ablation in sapphire the observed gentle etch phase is subject to non-thermal **and** thermal mechanism(s). Discrimination between the two is demonstrated in the different dynamics. Thermal mechanism(s) dominate, especially for semi-conductive and metallic surfaces. Thin transparent layers of films, such as ITO or PANI on photo-resists, can be removed selectively using ultrashort laser pulses in the IR.

ACKNOWLEDGEMENTS Part of this work conducted by the LMTB GmbH has been supported by the Berlin Senate, co-financed by the European Union (EFRE).

REFERENCES

1 E.E.B. Campbell, D. Ashkenasi, A. Rosenfeld: *Lasers in Materials Science* (Trans Tech Publications, Switzerland 1999) pp. 123–144 (1997)
2 K. Itoh, W. Watanabe, K. Yamada, D. Kuroda: Opt. Lett. **26**, 1912 (2001)
3 D. Bäuerle (Ed.): *Laser Processing and Chemistry,* 3rd edn. (Springer, Berlin, New York 2000) Chapt. 13
4 F. Korte, S. Adams, A. Egbert, C. Fallnich, A. Ostendorf: Opt. Exp. **7**, 41 (2000)
5 D. Ashkenasi, G. Herbst, A. Rosenfeld, H. Varel, M. Lorenz, R. Stoian, E.E.B. Campbell: Proc. SPIE **3343**, 400 (1998)
6 B.C. Stuart, M.D. Feit, A.M. Rubenchik, B.W. Shore, M.D. Perry: Phys. Rev. Lett. **74**, 2248 (1995)
7 D. Ashkenasi, A. Rosenfeld, H. Varel, M. Wahmer, E.E.B. Campbell: Appl. Surf. Sci. **120**, 65 (1997)
8 R. Stoian, D. Ashkenasi, A. Rosenfeld, E.E.B. Campbell: Phys. Rev. B **62**, 13 167 (2000)
9 R. Stoian, D. Ashkenasi, A. Rosenfeld, E.E.B. Campbell: Phys. Rev. Lett. **88**, 9 (2002)
10 D. Ashkenasi, R. Stoian, A. Rosenfeld: Appl. Surf. Sci. **154–155**, 40 (2000)
11 B.C. Stuart, M.D. Feit, S. Herman, A.M. Rubenchik, B.W. Shore, M.D. Perry: Phys. Rev. B **53**, 1749 (1996)
12 F. Quèrè, S. Guizard, P. Martin et al.: Appl. Phys. B **68**, 459 (1999)
13 K. Sokolowski-Tinten, D. v.d. Linde: Phys. Rev. B **61**, 2643 (2000)
14 D. v.d. Linde, H. Schüler: J. Opt. Soc. Am. B **13**, 216 (1996)
15 S. Guizard et al.: J. Phys.: Condens. Matter **5**, 7033 (1993)
16 S.C. Jones, A.H. Fischer, P. Braunlich, P. Kelly: Phys. Rev. B **37**, 755 (1988)
17 R.C. Hughes: Phys. Rev. B **19**, 5318 (1979)
18 A. Miotello, M. Dapor: Phys. Rev. B **56**, 2241 (1997)
19 E.M. Logothesis, P.L. Hartman: Phys. Rev. Lett. **18**, 581 (1997)
20 J.H. Bechtel, W.L. Smith, N. Bloembergen: Phys. Rev. B **15**, 4557 (1977)
21 S.-S. Wellershof, J. Hohlfeld, J. Guedde, E. Matthias: Appl. Phys. A **69**, S99 (1999)
22 R. Kelly: A. Miotello: Appl. Surf. Sci. **96–98**, 205 (1996)
23 L.V. Zhigilei, P.B.S. Kodali, B.J. Garrison: Chem. Phys. Lett. **276**, 269 (1997)
24 R. Stoian, H. Varel, A. Rosenfeld, D. Ashkenasi, E.E.B. Campbell, R. Kelly: Appl. Surf. Sci. **165**, 44 (2000)
25 O. Yavas, C. Ochiai, M. Takai: Appl. Phys. A **69** [Suppl.], 875 (1999)
26 R. Haight, D. Hayden, P. Longo, T. Neary, A. Wagner: J. Vac. Sci. Technol. B **17**, 3137 (1999)
27 D. Ashkenasi, A. Rosenfeld: Proc. SPIE **4637**, 169 (2002)
28 H. Varel, D. Ashkenasi, A. Rosenfeld, R. Herrmann, F. Noack, E.E.B. Campbell: Appl. Phys. A. **62**, 293 (1996)
29 C.B. Schaffer, A. Brodeur, J.F. Garcia, E. Mazur: Opt. Lett. **26**, 93 (2001)